The presence of CH_3NH_2 neutral species in organometal halide perovskite films

Min-Cherl Jung,[1] Young Mi Lee,[2] Han-Koo Lee,[2] Jinwoo Park,[3] Sonia R. Raga,[1] Luis K. Ono,[1] Shenghao Wang,[1] Matthew R. Leyden,[1] Byung Deok Yu,[4] Suklyun Hong,[3] and Yabing Qi[1,a)]

[1]*Energy Materials and Surface Sciences Unit (EMSS), Okinawa Institute of Science and Technology Graduate University (OIST), 1919-1 Tancha, Onna-son, Okinawa 904-0495, Japan*
[2]*Pohang Accelerator Laboratory, POSTECH, Pohang 790-784, South Korea*
[3]*Graphene Research Institute and Department of Physics, Sejong University, Seoul 143-747, South Korea*
[4]*Department of Physics, University of Seoul, Seoul 130-743, South Korea*

(Received 15 December 2015; accepted 2 February 2016; published online 17 February 2016)

We report the presence of CH_3NH_2 neutral species not only on the surface but also at grain boundaries in the interior of thin polycrystalline films of methylammonium lead iodide perovskite $CH_3NH_3PbI_3$ (thickness ~ 50 nm) that were prepared using a standard solution method. Different chemical states for C *K*-edge were observed at the surfaces and in the interiors of perovskite films. Salient features of $\sigma^*(CH_3\text{-}NH_3^+$: methylammonium cation) and $\sigma^*(CH_3\text{-}NH_2$: methylamine neutral species) were observed at 290.3 and 292.8 eV in both partial (surface-sensitive) and total (bulk) electron yield modes by near-edge x-ray absorption fine structure measurements. Consistently, two chemical states originated from $CH_3NH_3^+$ and CH_3NH_2 in C 1*s* and N 1*s* core-level spectra were observed using high-resolution x-ray photoelectron spectroscopy. Using density functional theory calculations, we show that CH_3NH_2 cannot reside stably in the $MAPbI_3$ perovskite crystal structure. Therefore, we propose that these CH_3NH_2 neutral species are mainly located on the surface or at grain boundaries in the interior of $CH_3NH_3PbI_3$ films.
[http://dx.doi.org/10.1063/1.4941994]

Solar cells based on organometal halide perovskite have been evolving rapidly. The newly achieved efficiencies exceeding 20%[1] make perovskite solar cells a promising candidate to compete with even the highest efficiency single crystal Si cells.[2–5] Organometal halide perovskite shows several attractive properties for photovoltaic applications, such as wide absorption photon range ($\sim$800 nm),[2] weak exciton-binding energy (<50 meV),[6] and high carrier mobilities (electron ~ 8 and hole $\sim 12\,cm^2/V\,s$).[7,8] To further improve device performance, it is crucial to understand the exact chemical structure and the precise role of each interface in devices.[9] Especially, several research groups studied the role of the organic cation $CH_3NH_3^+$ for a better understanding about the material stability and degradation mechanism.[10,11] Although a few theoretical studies have been reported,[12–14] experimental studies are somewhat lagging behind. If we understand the exact chemical structure and the precise role of each interface in perovskite solar cells, we can establish an optimized fabrication method, taking into consideration necessary interface treatment on electron and hole transport layers, minimizing degradation factors, optimized material design, etc.

In this study, we used near-edge x-ray absorption of fine structure (NEXAFS) and high-resolution x-ray photoelectron spectroscopy (HRXPS) with synchrotron radiation to understand the exact chemical structure of organometal halide perovskite at the surface as well as in the interior of the bulk film. We found the presence of CH_3NH_2 neutral species at surface and in the interiors of organometal halide perovskite. Based on our experimental results and density functional theory calculations, we propose that the neutral CH_3NH_2 species mainly reside either on the surface or at grain boundaries in the interior of $CH_3NH_3PbI_3$ films.

The patterned, fluorine-doped tin oxide glass (FTO Pilkington, 7 Ω/□) was prepared with HCl and Zn powder and cleaned. On this substrate, we deposited a 100-nm layer of compact layer (cl) of TiO_2 using spray pyrolysis with a precursor solution of acetylacetone, Ti (IV) isopropoxyde, and anhydrous ethanol (3:3:2) and then performed post-annealing at 480 °C on a hotplate. Basically, perovskite thin film fabrication followed a modified version of the two-step method of Burschka *et al.*[15] First, a solution of PbI_2 in dimethylformamide (460 mg ml^{-1}) was prepared and stirred at 70 °C for $\geq$2 h. We performed spin-coating at 6000 rpm for 30 s on the cl-TiO_2 substrates, previously heated at 70 °C. After the spin coating, the PbI_2 layer was dried at 70 °C for 20 min. Then, a 20 mg/ml methylammonium iodide (MAI) solution in 2-propanol (IPA) was prepared and kept at 70 °C. PbI_2 films were dipped in the MAI solution for 30 s with gentle shaking of the substrates. After dipping, substrates were rinsed in copious IPA and dried immediately by spinning them on a spin-coater, after which they were annealed for 20 min on the hot plate at 70 °C. To confirm the film thickness and surface morphology, we used an AFM (MFP-3D Asylum Research) and scanning electron microscopy (Quanta 250 FEG, FEI). X-ray diffraction (D8 Discover, Bruker Corporation) and UV-Vis spectrophotometry (Evolution 600 UV-Vis spectrophotometer, Thermo Scientific) were used to determine the crystalline

a)Author to whom correspondence should be addressed. Electronic mail: Yabing.Qi@OIST.jp

structure and optical bandgap, respectively. All NEXAFS measurements were performed at room temperature and at the beamline 4D of Pohang Light Source II (PLS II), Korea. We used the total electron yield (TEY) and partial electron yield (PEY) detection mode for NEXAFS spectra by recording the sample current normalized to a signal current, which was measured simultaneously using a gold mesh in ultrahigh vacuum ($<10^{-9}$ Torr). In this case, a *p*-polarized (≈85%) synchrotron photon beam, with an energy in the range of 279–320 eV and a spectral energy resolution of ΔE = 150 meV, had probing depths of 6 nm and 25 nm, for PEY and TEY modes, respectively. For HRXPS measurements, we performed two experiments using synchrotron radiation (52–860 eV) and a monochromated Al*K*α (1486.6 eV) source. HRXPS spectra were obtained at the 10D HRXPS beamline of PLSII. Photon energy was varied from 50 eV to 860 eV to obtain high-quality XPS spectra. Photoelectron signals were recorded with a PHOIBOS 150 electron energy analyzer equipped with a two-dimensional charge-coupled device (2D CCD) detector (Specs GmbH), collecting photoelectrons from the surface normal. The base pressure of the main chamber was maintained below 9.8×10^{-11} Torr. In the case of lab source, we used the monochromated Al*K*α (1486.6 eV) and a multi-channel plate analyzer with 180° hemispherical and 165 mm mean radii in the AXIS Ultra DLD (Kratos Surface Analysis). The energy resolution was <0.5 eV in both techniques. Chemical states of all samples were obtained measuring the valence region and the Pb 4*f*, I 3*d*, C 1s, and N 1*s* core-levels spectra. O 1*s* core-level was also measured to monitor any contamination during the sample transfer. O 1*s* core-level intensity was below the detection limits of the instruments. Binding energies were calibrated with reference to the Au $4f_{7/2}$ level (84.0 eV).[16] We fitted both C and N 1*s* core-level peaks using Doniach-Sŭnjić curves convoluted with Gaussian distribution of 0.5 eV full-width at half-maximum.[17] Background due to inelastic scattering was subtracted by the Shirley (or integral) method.[18] All calculations were performed using density functional theory (DFT) as implemented in the code of the CASTEP.[19] We used ultrasoft Vanderbilt-type pseudopotentials[20] and the exchange-correlation functional of the Perdew-Burke-Ernzerhof expression revised for solids (PBEsol) in the generalized gradient approximation (GGA).[21,22] Electronic wave functions were expanded by plane waves with an energy cut-off of 280 eV. The k-space integration was performed using a $3 \times 3 \times 1$ mesh in the Brillouin zone (BZ) of a three-dimensionally periodic $3 \times 3 \times 1$ supercell. The geometry optimization for the tetragonal phase was carried out until the Hellmann-Feynman force acting on the atoms was smaller than 0.03 eV/Å. To obtain the most stable atomic structure for $(CH_3NH_3,CH_3NH_2)PbI_3$, various initial atomic configuration were considered and all the atoms in the supercell were fully relaxed without any symmetry constraint. Also, we used the Mulliken charge analysis method to analyze charge populations. The binding energy E_{safe} had the following form:

$$E^{m,n}_{binding} = E^{m,n}_{total} - E_{PbI_3} - m \times E_{CH_3NH_3} - n \times E_{CH_3NH_2},$$

$$E^{CH_3NH_3}_{binding} = (E^{total}_{CH_3NH_3+PbI_3} - E_{PbI_3} - 16 \times E_{CH_3NH_3})/16,$$

$$E^{CH_3NH_2}_{binding} = (E^{total}_{CH_3NH_2+PbI_3} - E_{PbI_3} - 16 \times E_{CH_3NH_2})/16,$$

$$E^{m,n}_{binding'} = m \times E^{CH_3NH_3}_{binding} + n \times E^{CH_3NH_2}_{binding},$$

$$E_{safe} = E^{m,n}_{binding} - E^{m,n}_{binding'},$$

where *m* is the number of CH_3NH_3 molecules, *n* is the number of CH_3NH_2 molecules, $E^{m,n}_{binding}$ is the binding energy of CH_3NH_3 molecule m and CH_3NH_2 molecule n in the PbI_3 $3 \times 3 \times 1$ unit cell, $E^{m,n}_{total}$ is the total energy of CH_3NH_3 molecule m and CH_3NH_2 molecule n in the PbI_3 $3 \times 3 \times 1$ unit cell, E_{PbI_3} is the total energy of the PbI_3 $3 \times 3 \times 1$ unit cell, $E_{CH_3NH_3}$ is the energy of CH_3NH_3 single molecule, $E_{CH_3NH_2}$ is the energy of CH_3NH_2 single molecule, $E^{CH_3NH_3}_{binding}$ is the binding energy of CH_3NH_3 single molecule, $E^{CH_3NH_2}_{binding}$ is the binding energy of CH_3NH_2 single molecule, $E^{total}_{CH_3NH_3+PbI_3}$ is the total energy of 16 CH_3NH_3 molecules in the PbI_3 $3 \times 3 \times 1$ unit cell, and $E^{total}_{CH_3NH_2+PbI_3}$ is the total energy of 16 CH_3NH_2 molecules in the PbI_3 $3 \times 3 \times 1$ unit cell

In these forms, we considered various ratios of CH_3NH_3 and CH_3NH_2 molecules in the tetragonal-phase PbI_3 structure with 16 kinds of mixing conditions. In the equation, negative and positive values of E_{safe} represent stable and unstable structures of $(CH_3NH_3,CH_3NH_2)PbI_3$, respectively.

The solution-prepared $CH_3NH_3PbI_3$ ($MAPbI_3$) film was measured by NEXAFS with synchrotron radiation. We measured both partial (PEY, probing-depth of ∼6 nm) and total electron yield (TEY, ∼25 nm) modes to see whether electronic structure differed between surface and bulk organometal halide perovskite.[23] Different chemical states are observed only in PEY mode (Figure 1(a)) at the binding energy of ∼285 eV. The rest of the spectra are almost the same between the PEY and TEY mode measurements in solution-prepared $MAPbI_3$. The most significant absorption features are the two shoulders at the binding energy of ∼290 eV (Figure 1(a)). To understand these surface and bulk features, we performed curve-fittings for both of them (Figure 1(b)). We found σ*(CH_3-NH_3^+), σ*(CH_3-NH_2), and σ*(C*=C) at 290.3, 292.8, and 301.4 eV in both measurements.[23] The carbon chemical states C*-M (Metal) and π* (C*=C) were found at 282.9 and 285.5 eV in the PEY mode.[23] In the TEY mode, however, we could not observe any of these chemical states in the energy range from 280.0 to 285.5 eV.

The photoelectron escaping depth in a thin film depends on the energy of incident photons.[24] To investigate chemical structure differences between surface and bulk, we performed high-resolution x-ray photoelectron spectroscopy with synchrotron radiation and a monochromated Al *K*α source. The Pb $4f_{7/2}$ and I $4d_{5/2}$ core-levels spectra at binding energies of 138.7 and 49.7 eV show no significant change in chemical states or shapes for all photon energies measured (Figure 2(a)). There is only a single chemical state for each of these peaks. In the case of C 1*s* core-level spectra, however, we observed different shapes when different incident photon energies (370, 620, and 1486.7 eV) were used (Figure 2(b)). Using photo energy of 370 eV, the C 1*s* core-level spectrum shows some tail states around 282.5 eV that do not appear in the case of 620 or 1486.7 eV photon energy. The escaping depth of photoelectrons (inelastic mean free path) with a photon energy of 370 eV is ∼1 nm, while the escaping depth for 620 or

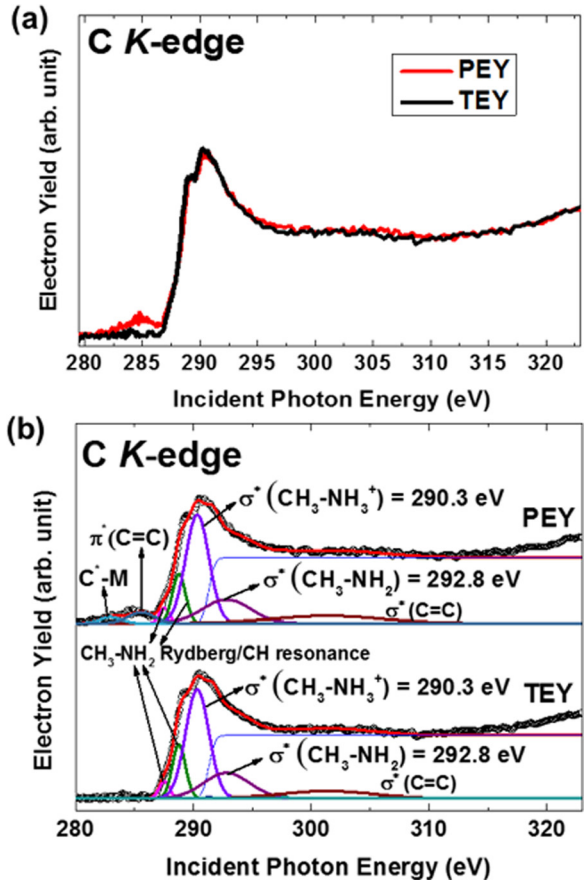

FIG. 1. Observation of two organic elements in the bulk and surface of perovskite and their differences in chemical states. (a) C *K*-edge NEXAFS in PEY (surface sensitivity) and TEY (bulk sensitivity) modes. The photon energy peak at 285 eV and two significant peaks around 290 eV are apparent. (b) Curve-fitting data.

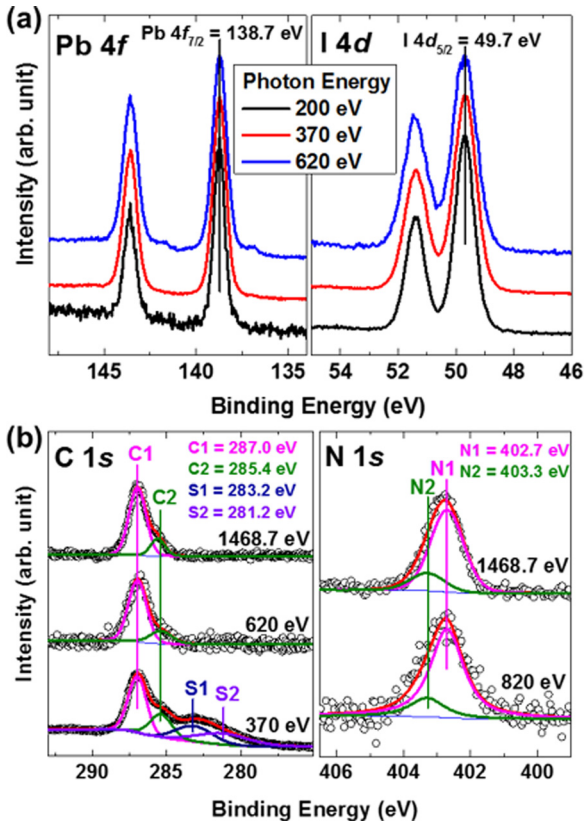

FIG. 2. HRXPS measurements with synchrotron radiation. (a) Pb 4*f* and I 4*d* core-level spectra measured at various photon energies. No changes of Pb 4*f* and I 4*d* chemical states are observed at different photon energies. (b) C and N 1*s* core-levels spectra with various photon energies and after the optimized curve-fitting analysis. C1, N1 and C2, N2 were assigned to CH_3-NH_3^+ and CH_3-NH_2 chemical states, respectively. S1 and S2 are species corresponding to carbon metallic chemical states.

1486.7 eV are ~2 nm and ~5 nm, respectively.[24] The presence of these tail states only for low photon energy of 370 eV suggests that these tail states are associated with the surface of the solution-prepared $MAPbI_3$ thin film. In the case of N 1*s* core-level spectra, we could not observe any significant surface states (Figure 2(b)). To understand chemical states of C and N 1*s* core-levels, we performed curve fittings and obtained several chemical states of C1 (287 eV), C2 (285.4 eV), S1 (283.2 eV), S2 (281.2 eV), N1 (403.3 eV), and N2 (402.7 eV) (Figure 2(b)). We propose that the chemical states of C1, N1 and C2, N2 are from CH_3-NH_3^+ and CH_3-NH_2.[25,26] S1 and S2 are originated from the surface states of C*-M (Metal) and C*=C bonding.[27,28] These HRXPS results are consistent with the NEXAFS results.

Finally, we found CH_3NH_2 in the organometal halide perovskite with different chemical states between bulk and surface. On the other hand, Pb and I exhibited the same single chemical states in both locations. If CH_3NH_2 resides inside the perovskite crystal structure, it is expected to introduce more than one chemical states of Pb or I. To determine the location of CH_3NH_2 in the perovskite, we performed the air exposure experiment (Figure S2 in the supplementary material).[29] It has been reported that water (H_2O) in air degrades perovskite.[30,31] Specifically, $CH_3NH_3^+$ becomes CH_3NH_2.[30,31] If the C1 and C2 chemical states are originated from $CH_3NH_3^+$ and CH_3NH_2, respectively, it is expected that the ratio between C1 and C2 intensities decreases after air exposure. We performed the air exposure experiment at 24 °C and 30% humidity and then measured the sample with HRXPS after 1 and 3 days (Figure S2 in the supplementary material).[29] Indeed, the ratio between C1 and C2 intensities decreased after air exposure (Figure S2 in the supplementary material),[29] which is consistent with the proposal that the C2 chemical state is originated from CH_3NH_2 neutral species.

Based on these experimental observations, we propose that CH_3NH_2 exists in solution-prepared organometal halide perovskites. In addition, one important question arises regarding the location of CH_3NH_2 in $CH_3NH_3PbI_3$ films. Therefore, we further investigated the charge populations, density of states (DOS), and system stability of CH_3NH_3 and CH_3NH_2 molecules in PbI_3 using DFT-based simulations. In these calculations, we considered the tetragonal-phase PbI_3 structure (Figure 3(a)).[32] First, we investigated the atomic charge states and the C-N bond length of the isolated CH_3NH_3 and CH_3NH_2 molecules (Figure 3(b)). Basically, negative or positive values of charge populations are represented by electron accumulation or depletion relative to what it had. Charge populations of CH_3NH_3 and CH_3NH_2 molecules are changed in the tetragonal-phase PbI_3 in comparison with those of isolated CH_3NH_3 and CH_3NH_2 (Figures 3(c) and 3(d)). In particular, the change of charge population of I atoms is very sensitive to the presence of CH_3NH_3 or CH_3NH_2 molecules in PbI_3. We used the binding energies

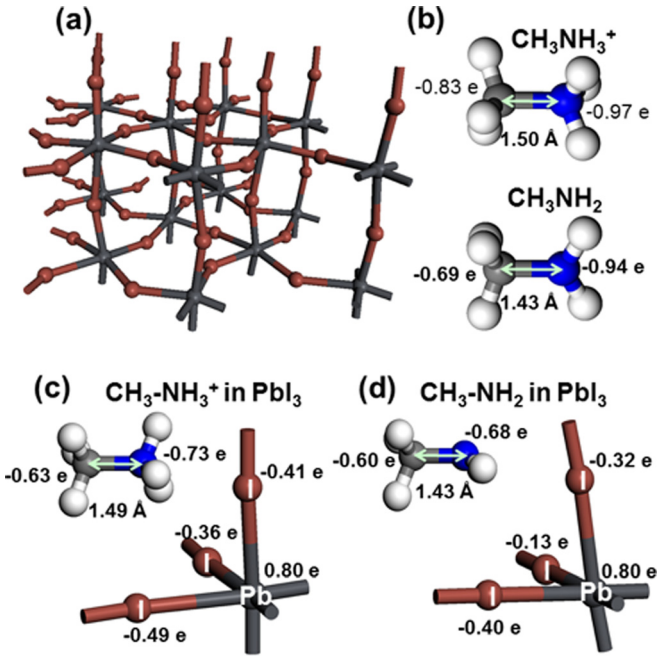

FIG. 3. Geometry-optimized atomic structures for PbI_3 (a), isolated CH_3NH_3 and CH_3NH_2 molecules (b), $CH_3NH_3PbI_3$ (c), and $CH_3NH_2PbI_3$ (d). In (b)–(d), charge states of C, N, Pb, and I are also shown using a Mulliken population analysis. It is noted that distinct chemical states of I are observed when CH_3NH_2 is bonded to the PbI_3 structure.

(E_{safe}) for the stability of possible structures when CH_3NH_3 and CH_3NH_2 coexist in PbI_3 (Table S1 in the supplementary material).[29] The calculated results of E_{safe} show positive values for all configurations of (CH_3NH_3, CH_3NH_2)PbI_3. This indicates that CH_3NH_2 is unstable in the interior region of PbI_3, and instead, it should be located at grain boundaries of thin polycrystalline films of $CH_3NH_3PbI_3$. In this case, CH_3NH_2 cannot directly interact with the basic building blocks of PbI_3. This conclusion is consistent with the experimental observation of a single chemical state for Pb and I in HRXPS measurements. In addition, DFT calculations of the DOS show different band gaps for $CH_3NH_3PbI_3$ and $CH_3NH_2PbI_3$; the band gap of $CH_3NH_3PbI_3$ was ~1.70 eV, while $CH_3NH_2PbI_3$ exhibits no band gap (Figure S3 in the supplementary material).[29] The DFT result of $CH_3NH_2PbI_3$ with no band gap is inconsistent with the experimental result of optical band gap of ~1.55 eV (Figure S1 in the supplementary material).[29] This also suggests that CH_3NH_2 cannot reside stably inside the $CH_3NH_3PbI_3$ crystal structure, but rather resides mainly on the surface or at grain boundaries in the interior of thin polycrystalline films of $CH_3NH_3PbI_3$. A direct correlation between the concentration of CH_3NH_2 in perovskite cells and their solar cell performance would be particularly helpful. But, unfortunately, it is challenging to accurately determine the total concentration of CH_3NH_2 for a bulk film of perovskite with a typical thickness of ~300 nm as those used in perovskite solar cells. Nevertheless, such a correlation can be partially inferred by the study that investigated the effects of annealing conditions on perovskite solar cell performance.[33] In that study, the solar-cell efficiency of 10.7% was obtained for perovskite solar cells using perovskite films with post-annealing at 115 °C in N_2 environment, while the efficiency was substantially lower (6.7%) with post-annealing at 105 °C.[33] Note that the two types of perovskite solar cells were otherwise prepared in an identical way. Presumably, post-annealing at 105 °C was not sufficient to remove the majority of CH_3NH_2 from the perovskite film and, therefore, could be a likely cause responsible for the lower efficiency.[33] Regarding the origin of CH_3NH_2, it is possible that after perovskite films are prepared, a certain amount of unreacted CH_3NH_3I still remains in perovskite films even after annealing. CH_3NH_3I can further decompose to CH_3NH_2, leading to the presence of CH_3NH_2 in perovskite films. In addition, when $CH_3NH_3PbI_3$ perovskite films degrade, CH_3NH_2 can also be generated as a product, which can be another origin of CH_3NH_2 in perovskite films.

In conclusion, we found CH_3NH_2 neutral species on the surface and in the interior of $CH_3NH_3PbI_3$ films prepared using a typical solution method. Based on the experimental results and density functional theory calculations, we conclude that the CH_3NH_2 neutral species is mainly located on the surface or at grain boundaries in the interior of $CH_3NH_3PbI_3$ films, which is expected to affect device performance and degradation. The observation of different chemical states on the surface of $CH_3NH_3PbI_3$ films such as C-metal and C*=C bonding is also discussed.

This work was supported by funding from the Energy Materials and Surface Sciences Unit of the Okinawa Institute of Science and Technology Graduate University and JSPS KAKENHI Grant No. 15K17925. Y.M.L and H.-K.L are grateful for financial support from the Basic Science Research Program of the National Research Foundation of Korea (NRF) funded by the Ministry of Education (NRF-2015R1C1A2A01054543 and NRF-2011-0006744). The experiment at the PLSII was supported, in part, by MEST and POSTECH. Calculations were supported by the Nano Material Technology Development Program (2012M3A7B4049888) through the National Research Foundation of Korea (NRF) funded by the Ministry of Science, ICT and Future Planning (MSIP), and the Priority Research Center Program (2010-0020207) through NRF funded by the Ministry of Education (MOE). The authors thank Steven D. Aird, the Technical Editor at Okinawa Institute of Science and Technology Graduate University (OIST) for valuable suggestions in revising the manuscript.

[1]W. S. Yang, J. H. Noh, N. J. Jeon, Y. C. Kim, S. Ryu, J. Seo, and S. I. Seok, Science **348**, 1234 (2015).
[2]M. A. Green, A. Ho-Baillie, and H. J. Snaith, Nat. Photonics **8**, 506 (2014).
[3]M. Grätzel, Nat. Mater. **13**, 838 (2014).
[4]W. Nie, H. Tsai, R. Asadpour, J.-C. Blancon, A. J. Neukirch, G. Gupta, J. J. Crochet, M. Chhowalla, S. Tretiak, M. A. Alam, H.-L. Wang, and A. D. Mohite, Science **347**, 522 (2015).
[5]S. D. Stranks and H. J. Snaith, Nat. Nanotechnol. **10**, 391 (2015).
[6]V. D'Innocenzo, G. Grancini, M. J. P. Alcocer, A. R. S. Kandada, S. D. Stranks, M. M. Lee, G. Lanzani, H. J. Snaith, and A. Petrozza, Nat. Commun. **5**, 3586 (2014).
[7]C. Wehrenfennig, G. E. Eperon, M. B. Johnston, H. J. Snaith, and L. M. Herz, Adv. Mater. **26**, 1584 (2013).
[8]C. Motta, F. El-Mellouhi, and S. Sanvito, Sci. Rep. **5**, 12746 (2015).
[9]M. A. Loi and J. C. Hummelen, Nat. Mater. **12**, 1087 (2013).
[10]W. J. Yin, T. Shi, and Y. Yan, Adv. Mater. **26**, 4653 (2014).

[11]J. M. Azpiroz, E. Mosconi, J. Bisquert, and F. De Angelis, Energy Environ. Sci. **8**, 2118 (2015).
[12]Y. Wang, T. Gould, J. F. Dobson, H. Zhang, H. Yang, X. Yao, and H. Zhao, Phys. Chem. Chem. Phys. **16**, 1424 (2013).
[13]A. Buin, R. Comin, J. Xu, A. H. Ip, and E. H. Sargent, Chem. Mater. **27**, 4405 (2015).
[14]I. E. Castelli, J. M. García-Lastra, K. S. Thygesen, and K. W. Jacobsen, APL Mater. **2**, 081514 (2014).
[15]J. Burschka, N. Pellet, S.-J. Moon, R. Humphry-Baker, P. Gao, M. K. Nazeeruddin, and M. Grätzel, Nature **499**, 316 (2013).
[16]C. D. Wagner, W. M. Riggs, L. E. Davis, and J. F. Moulder, *Handbook of X-Ray Photoelectron Spectroscopy, a Reference Book of Standard Data for Use in X-Ray Photoelectron Spectroscopy* (Perkin–Elmer Corp., 1979).
[17]S. Doniach and M. Sunjic, J. Phys. C: Solid State Phys. **3**, 285 (1970).
[18]D. A. Shirley, Phys. Rev. B **5**, 4709 (1972).
[19]S. J. Clark, M. D. Segall, C. J. Pickard, P. J. Hasnip, M. I. J. Probert, K. Refson, and M. C. Payne, Z. Kristallogr **220**, 567–570 (2005).
[20]D. Vanderbilt, Phys. Rev. B **41**, 7892 (1990).
[21]J. P. Perdew, A. Ruzsinszky, G. I. Csonka, O. A. Vydrov, G. E. Scuseria, L. A. Constantin, X. Zhou, and K. Burke, Phys. Rev. Lett. **100**, 136406 (2008).
[22]F. Brivio, A. B. Walker, and A. Walsh, APL Mater. **1**, 042111 (2013).
[23]J. Stöhr, *NEXAFS Spectroscopy*, Springer Series in Surface Sciences Vol. 25 (Springer, 1992).
[24]D. Briggs and M. P. Seah, *Practical Surface Analysis, Auger and X-ray Photoelectron Spectroscopy* (Wiley, 1990).
[25]A. P. Dementjev, A. de Graaf, M. C. M. van de Sanden, K. I. Maslakov, A. V. Naumkin, and A. A. Serov, Diamond Relat. Mater. **9**, 1904 (2000).
[26]S. Bhattacharyya, C. Cardinaud, and G. Turban, J. Appl. Phys. **83**, 4491 (1998).
[27]G. Deniau, L. Azoulay, P. Jégou, G. Le Chevallier, and S. Palacin, Surf. Sci. **600**, 675 (2006).
[28]U. Gelius, P. F. Hedén, J. Hedman, B. J. Lindberg, R. Manne, R. Nordberg, C. Nordling, and K. Siegbahn, Phys. Scr. **2**, 70 (1970).
[29]See supplementary material at http://dx.doi.org/10.1063/1.4941994 for the sample fabrication, characterization, air-exposure result, and bandgap calculation.
[30]J. M. Frost, K. T. Butler, F. Brivio, C. H. Hendon, M. van Schilfgaarde, and A. Walsh, Nano Lett. **14**, 2584 (2014).
[31]Y. Han, S. Meyer, Y. Dkhissi, K. Weber, J. M. Pringle, U. Bach, L. Spiccia, and Y.-B. Cheng, J. Mater. Chem. A **3**, 8139 (2015).
[32]T. Baikie, Y. Fang, J. M. Kadro, M. Schreyer, F. Wei, S. G. Mhaisalkar, M. Graetzel, and T. J. White, J. Mater. Chem. A **1**, 5628 (2013).
[33]S. R. Raga, M.-C. Jung, M. V. Lee, M. R. Leyden, Y. Kato, and Y. B. Qi, Chem. Mater. **27**, 1597 (2015).